This is a preprint, the final version is subject to change, of the American Mineralogist (MSA)
Cite as Authors (Year) Title. American Mineralogist, in press.
(DOI will not work until issue is live.) DOI: http://dx.doi.org/10.2138/am.2014.4311

Revision 2

Fluorescence of Trivalent Neodymium in Various Materials Excited by a 785-nm Laser

Hongmei Chen and Richard W.Stimets
Department of Physics, University of Massachusetts Lowell, Lowell, Massachusetts 01854 U.S.A.

ABSTRACT

The nature of the fluorescence in the frequency-shift range of 1000-2500 cm^{-1} observed in the Raman spectra of many minerals when excited by a 785-nm laser has been investigated. Among the trivalent rare earths only Nd^{3+} has the combination of a good ionic-radius match to substitute for Ca^{2+} and an arrangement of energy levels to produce fluorescence in the frequency-shift range of interest. Raman/fluorescence spectra of six calcium-based minerals, namely fluorite, calcite, powellite, scheelite, apatite, and grossular/tsavorite, have been obtained at both room temperature and liquid-nitrogen temperature and transition assignments made for the majority of fluorescence lines in fluorite, powellite, scheelite, and grossular/tsavorite. The room-temperature results agree closely with results on individual minerals obtained by previous workers for fluorite and scheelite. The liquid-nitrogen-temperature results as well as the transition assignments for powellite and grossular/tsavorite are new. The Nd concentration has been measured by laser-ablation induction-coupled-plasma mass spectrometry (LA-ICP-MS) and correlated with Nd^{3+} fluorescence intensity where possible. For fluorite, the fluorescence intensity increases at least linearly with concentration at levels up to a few ppm and then saturates at higher levels due to concentration quenching. Analysis of room-temperature Raman/fluorescence spectra of a much larger group of minerals available on the RRUFF website shows that strong or

This is a preprint, the final version is subject to change, of the American Mineralogist (MSA)
Cite as Authors (Year) Title. American Mineralogist, in press.
(DOI will not work until issue is live.) DOI: http://dx.doi.org/10.2138/am.2014.4311

very strong Nd^{3+} fluorescence is much more likely in calcium-based minerals than in non-calcium-based ones and is completely absent for minerals containing iron in the chemical formula. Nd^{3+} fluorescence is best understood in fluorite and less well understood in the other five minerals. Further study of calcite, apatite and grossular/tsavorite is necessary to improve the understanding of the charge-compensation mechanisms and increase the number of identified transitions in calcite and apatite. The results of this work indicate that Nd^{3+} fluorescence in calcium-based minerals, when excited by a 785-nm laser, has potential uses in three areas: mineral identification, structure characterization and determination of trace-element concentration.

Keywords: Raman spectrum fluorescence, neodymium fluorescence, rare-earth impurities in minerals, laser-ablation induction-coupled-plasma mass spectrometry, LA-ICP-MS

INTRODUCTION

Raman spectroscopy in mineral identification

Raman spectroscopy is widely used in the identification of minerals and gems because each particular chemical species has a unique Raman spectrum, which is the result of its chemical composition and crystal structure. The technique is particularly useful for distinguishing members of a series in which the Raman spectra are similar but show small but measurable differences in the positions of the spectral lines. In gem identification Raman scattering is a quick and non-destructive method of distinguishing authentic gemstones from cheaper imitations (Jenkins and Larsen, 2004)

In order to reduce unwanted fluorescence, the infrared 785-nm (sometimes 780-nm) titanium-sapphire laser is often used. However, even with the 785-nm laser, fluorescence is often observed and has generally been attributed to the presence of rare-earth impurities. In this paper we analyze the Raman/fluorescence spectra of a number of minerals excited by a 785-nm laser and give strong evidence that most of the observed fluorescence in the frequency–shift region of 1000-2500 cm^{-1} is due to the presence of a single type of rare-earth ion, namely Nd^{3+}. In some cases, the characteristic pattern produced by the crystal field is a reliable fingerprint of the host crystal and may itself be used for mineral identification where the true Raman spectrum is unreliable or masked by the fluorescence.

Energy levels of rare-earth ions

The 4f energy levels of four trivalent rare-earth ions are shown in Fig. 1. When a rare-earth ion is incorporated into a crystal as an impurity, the 2J+1 degenerate levels of the ionic multiplet are split by the crystal field by an amount of up to a few hundred cm^{-1}. For example, the ground state multiplet of Nd^{3+}, namely $^4I_{9/2}$ has 10 degenerate levels and in all site symmetries other than cubic is split into 5 doubly degenerate Kramers doublets. Also shown on the energy-level diagram are lines representing the transition energy produced by a 785-nm laser (12739 cm^{-1}). These lines lie close to some energy level of each of the four rare-earth ions, namely the $^4F_{5/2}$ level of Nd^{3+}, the $^6F_{5/2}$ level of Dy^{3+}, the $^4I_{9/2}$ level of Er^{3+}, and the $^3F_4$ level of Tm^{3+}. Absorption measurements of several samples of fluorite (CaF_2) containing Dy^{3+} indicate that the

785-nm laser energy is just slightly too energetic to lie within the $^6H_{15/2} \rightarrow {}^6F_{5/2}$ absorption band of Dy^{3+}. The match of laser energy to transition energy is better for Er^{3+} and Tm^{3+} but, in each case, non-radiative decay to the next-lowest 4f energy level, followed by subsequent fluorescence, would yield a frequency shift greater than 2500 cm^{-1}, which is outside of the range considered here. In Nd^{3+} the 785-nm laser excites the $^4I_{9/2} \rightarrow {}^4F_{5/2}$ transition. The excitation is followed by non-radiative relaxation to the $^4F_{3/2}$ multiplet and subsequent fluorescence to the ground state $^4I_{9/2}$ mutiplet. A non-cubic crystal field splits the $^4F_{3/2}$ multiplet into two doubly-degenerate levels so that there are 2*5=10 possible fluorescence lines between the $^4F_{3/2}$ and $^4I_{9/2}$ multiplets. Typically, due to weak transition strengths of some lines, fewer than 10 lines are actually observed. In the literature the five levels of the $^4I_{9/2}$ multiplet are referred to as Z_1-Z_5 and the two levels of the $^4F_{3/2}$ multiplet are referred to as R_1 and R_2. Among all of the trivalent rare earth ions, only Nd^{3+} has the required arrangement of energy levels to absorb the laser light and produce fluorescence in the frequency-shift range of 1000-2500 cm^{-1}.

Substitution of rare-earth ions as impurities

Substitution of rare-earth ions as impurities in minerals depends on having a close match of both ionic radius and charge between the rare-earth ion and the cation for which it is substituting. According to Goldschmidt's rules (Goldschmidt, 1926), free substitution can occur if the ionic radius differs by less than 15%, limited substitution can occur if the difference is 15-30% and little or no substitution can occur if the difference

is greater than 30%. The charge difference must not exceed 1. The rare-earth ionic radii exhibit the well-known lanthanide contraction, due to incomplete shielding by the 4f electrons. The ionic radius of Nd^{3+} (.983Å for six-fold coordination) is very close to that of Ca^{2+} (1.00 Å for six-fold coordination) (Withers et al., 2003). Thus Nd^{3+} can easily substitute for Ca^{2+} in many minerals. The necessary charge compensation can be provided by concurrent substitution of a lower valence cation, e.g. Si^{4+} for P^{5+}, or the addition of an extra anion such as F^- in an interstitial position. The compensation may be local, in which case it reduces the site symmetry of the Nd^{3+} impurity, or distant, in which case it does not.

Trivalent neodymium has both the required energy-level arrangement for 785-nm-excited fluorescence and the required ionic radius and minimal charge difference for ease of substitution for calcium, and it is the combination of these two properties which explain the widespread occurrence of fluorescence in the Raman/fluorescence spectra of calcium-based minerals.

EXPERIMENTAL EQUIPMENT AND METHODS

Raman/fluorescence spectrometer

Raman/fluorescence spectra covering the range of frequency shift from 200 cm^{-1} to 2500 cm^{-1} were obtained at both room temperature (294 K) and liquid nitrogen temperature (77 K) for all samples with an RSI-3000 spectrometer system, which operates in the backscattering geometry and has a spot size of less than 1 mm. The samples were placed in a 2.0-cm-diameter, 20-cm-long plastic tube with a funnel at the top to hold liquid nitrogen and surrounded by styrofoam insulation. A wad of aluminum

foil was placed around the sample on one side so that one face of the sample was close to the wall of the plastic tube and the sample remained in position when liquid nitrogen was poured in. A 3/8-inch-diameter access hole cut through the insulation allowed the experimenter to position the laser probe very close to the plastic-tube wall and within a few mm of the sample. The tight fit of the laser probe into the access hole prevented air from getting onto the cold plastic tube and causing condensation.

For each sample, a series of runs were first made at room temperature. Liquid nitrogen was poured in and several minutes were allowed to pass until the boiling quieted down. Then several runs were made at liquid nitrogen temperature. The fluorescence signal was strong enough so that a 10-second integration time was usually sufficient and typically eight runs were made and averaged to improve the signal–to-noise ratio. Because any motion of the sample between the two sets of runs was very small, the pairs of Raman/fluorescence spectra presented below can be assumed to come from the same part of the sample.

LA-ICP-MS system

The concentrations of all of the rare-earth elements, transition metals in the ranges Sc-Fe, Y-Mo, and La-W, as well as those of Ca, Sr, Ba and U were measured for all samples by the LA-ICP-MS system at the Graduate School of Oceanography at the University of Rhode Island. The system used a 230-nm pulsed ultraviolet laser operating at a repetition rate of 10 Hz which burned a hole at a rate of 2 μm/s for 60 s so that the hole depth was 120 μm. A hole diameter of 160 μm was used in most cases, except for some of the calibration samples, for which 80 μm was used. In order to determine the

This is a preprint, the final version is subject to change, of the American Mineralogist (MSA)
Cite as Authors (Year) Title. American Mineralogist, in press.
(DOI will not work until issue is live.) DOI: http://dx.doi.org/10.2138/am.2014.4311

true concentration of the elements, the values of the net count rate during the signal portion of the count rate curves were compared to those from NIST glass calibration samples. In the LA-ICP-MS technique it is important to choose isotopes so that a combination of isotopes of lower mass does not masquerade as a single isotope of higher mass. (See Kelley, 2006)

RAMAN/FLUORESCENCE SPECTRA I

Minerals chosen for study

Six calcium-based minerals which exhibit fluorescence in the spectral-shift region of 1000-2500 cm^{-1} were chosen for study in the present work. They are listed in Table 1 along with the source or location of origin, which is unknown in a few cases. Of the UML samples, the synthetic fluoride samples intentionally doped with Dy had been purchased from Optovac, Inc. many years ago. The undoped sample of CaF_2 was recently obtained from Fairfield Crystal Technology and is typical of their material sold as optical windows. The samples of calcite, powellite, scheelite, apatite and tsavorite were obtained from various mineral suppliers. The information on the RRUFF samples is listed on the RRUFF website. These samples had a variety of sources and locations of origin.

For each of the UML samples, peak positions and linewidths of both the observed Raman lines and Nd^{3+} fluorescence lines were determined, transition assignments were made, and the results were compared with those of previous work where possible. Each mineral is discussed individually below in this section. In the values for line position and energy level given in the figures and the tables below, the uncertainties are estimated to

This is a preprint, the final version is subject to change, of the American Mineralogist (MSA)
Cite as Authors (Year) Title. American Mineralogist, in press.
(DOI will not work until issue is live.) DOI: http://dx.doi.org/10.2138/am.2014.4311

be 1-2 cm^{-1}. In addition, the results from the UML samples are compared with the results from the RRUFF samples in the section entitled Raman/Fluorescence Spectra II.

Fluorite (CaF_2)

Fluorite has a cubic crystal structure (space group $Fm\bar{3}m$) and may be regarded as a simple cubic lattice of F^- ions with a Ca^{2+} ion at the center of every other cube. When Nd^{3+} substitutes for Ca^{2+} in CaF_2, the main mechanism by which the necessary charge compensation is accomplished is the incorporation of an interstitial F^-.

The local site symmetry of the Nd^{3+} impurity depends on the location of the F^-: full eightfold-coordinated cubic $m\bar{3}m$ (O_h) symmetry for remote compensation, tetragonal *4mm* (C_{4v}) symmetry for compensation at the central position of an adjacent cube along one of the crystal axes, and trigonal *3m* (C_{3v}) symmetry for compensation at the central position of an adjacent cube along a body diagonal.

The actual distribution of site symmetries of the Nd^{3+} ions in CaF_2 is probably a mixture of O_h, C_{4v} and C_{3v} as well as some sites containing Nd^{3+} clusters, which become important at high impurity levels. However, $4f \rightarrow 4f$ transitions in rare-earth ions, which are forbidden in the free ion, gain significant strength only when the local crystal field breaks the inversion symmetry. Thus, $4f \rightarrow 4f$ transitions of Nd^{3+} in CaF_2 are expected to be very weak at O_h sites, moderate at C_{3v} sites and strongest at C_{4v} sites because of the closeness of the charge-compensating F^- ion. It is the general consensus of

several studies over the years that the characteristic fluorescent spectrum of Nd^{3+} in CaF_2 presented below is due to Nd^{3+} ions at C_{4v} sites (Freeth and Jones, 1982; Payne et al. 1991).

Raman/fluorescence spectra were obtained for five samples of synthetic CaF_2 and two samples of natural CaF_2 and were all very similar. The spectra of a sample of CaF_2:0.05% Dy^{2+} are shown in Fig. 2. The Nd^{3+} fluorescence lines in the frequency-shift range of 1000-2000 cm^{-1} all narrow considerably at 77 K and three weak lines at 1044/1025 cm^{-1}, 1122/1107 cm^{-1} and 1775/1776 cm^{-1} decrease considerably in intensity. This decrease is a strong indication that these lines are due to transitions from the higher level (R_2) in the upper multiplet, which is significantly depopulated at 77 K. Having spectra at both 294 K and 77 K helps considerably in making transition assignments. Guided by previous results, most of the lines in Fig. 2 can be identified. Out of the ten possible transitions from R_m to Z_n, six are observed at 294 K and seven at 77 K. $R_2 \rightarrow Z_3$ is buried in the upper part of the much stronger peak due to $R_1 \rightarrow Z_2$. The two transitions $R_2 \rightarrow Z_4$ and $R_1 \rightarrow Z_4$ are apparently too weak to be observed.

A comparison of energy levels of Nd^{3+} in CaF_2 as deduced from the fluorescence spectra for previous work and the present work is given in Table 2 and generally shows very good agreement. The single significant discrepant value is that for the Z_5 level obtained by Kiss (1962). The reason for this discrepancy is not known. The previous results were obtained from samples of CaF_2 intentionally doped with Nd^{3+} for use as solid-state lasers. The present results show that the same fluorescence can occur in synthetic samples in which the Nd is an unintentional impurity at much lower

concentrations as well as in natural samples. Freeth and Jones (1982) analyzed their energy level values assuming C_{4v} site symmetry with a tetragonal crystal field having five parameters and including J-mixing, and obtained an excellent fit to the levels of the $^4I_{9/2}$ and $^4I_{11/2}$ multiplets with an rms deviation of 1.2 cm^{-1}. Clearly C_{4v} symmetry appears to be the dominant site symmetry for Nd^{3+} in CaF_2.

Both spectra also show several weak unidentified lines. Possible origins of these lines are fluorescence from Nd^{3+} at sites of symmetry other than C_{4v}, e.g. C_{3v} sites or Nd-cluster sites (See Payne et al. 1991). Their relatively low intensities indicate that either such sites are rarer than the C_{4v} sites and/or the line strengths are weaker. Overall, the Nd^{3+} fluorescence spectra of fluorite, although displaying some minor variations, are very similar and distinctive and are a reliable indicator that the host material is fluorite.

Calcite ($CaCO_3$)

Calcite has a rhombohedral crystal structure (space group $R\bar{3}c$) in which layers of Ca^{2+} ions alternate with layers of CO_3^{2-} molecular complexes. The Ca^{2+} has trigonal *3 (C_3)* site symmetry but previous fluorescence spectra of Nd^{3+} in calcite taken by Withers et al. (2003) indicate that the site symmetry of impurity atoms in calcite is not as distinct as it is with fluorite. The spectra reveal large inhomogeneous linewidths and smooth line profiles which are more characteristics of glassy hosts than crystalline ones. The authors attribute these features to a broad distribution of crystal-field environments caused by a variation in coordination number (6.6 ± 1), local lattice distortion, defects or other impurities.

Raman/fluorescence spectra were obtained for three samples of clear calcite, one sample of green calcite, and one sample of blue calcite. One sample of clear calcite and the sample of green calcite showed moderate or strong Nd^{3+} fluorescence. The fluorescence spectra of the clear calcite and the green calcite are quite different.

In the active sample of the clear calcite, the Nd^{3+} fluorescence was strong everywhere and showed a moderate variation (within a factor of two) over the sample. The fluorescence lines are in the range of frequency shift of 1100 cm^{-1} to 1840 cm^{-1}. Significant narrowing of the lines and reduction of the intensities of the transitions from the R_2 allows identification of seven of the ten transitions. It appears that most of the fluorescence spectrum arises from a dominant type of impurity site with a minor contribution from a second type of impurity site. The very narrow lines at 77 K indicate a high degree of crystalline order and low level of strain broadening.

In the sample of green calcite, the Nd^{3+} fluorescence was confined to a light brownish band about 1 mm thick that ran through the sample. The sharp drop off in fluorescence intensity with position away from the center of the band correlated strongly with a similar drop off in Nd concentration as measured by the LA-ICP-MS method. The Nd^{3+} fluorescence spectrum separates into two components: in the range of frequency shift of 1150 cm^{-1} to 1400 cm^{-1} a cluster of three lines at 294 K sharpens into four lines at 77 K, which can be identified as the four transitions from R_1/R_2 to Z_1/Z_2. In the range from 1450 cm^{-1} to 1700 cm^{-1} a broad peak does not sharpen and resolve at 77K, and it is not possible to make transition assignments.

It is clear that the Nd^{3+} fluorescence spectra show a much greater variation, both within an individual sample, and between different samples, than they do in fluorite. The

probable causes are a greater number of impurity site types as well as a greater variety of formation conditions. Further study with a larger number of calcite samples from different origins are necessary to determine whether may be a set of reliable characteristic Nd^{3+} fluorescence spectra for calcite. The results from the active sample of clear calcite in the present work indicate that such may be the case.

Powellite ($CaMoO_4$)

Powellite has a tetragonal crystal structure (space group $I4_1/a$), and the Ca^{2+} ions have a tetragonal $\bar{2}$ (S_4) site symmetry. Fluorescence of Nd^{3+} in powellite has been studied by Andrade et al. (2006) in a single crystal of $CaMoO_4$ doped with Nd^{3+} and co-doped with Nb^{5+} to investigate its use as a laser host, whose broad and intense absorption bands permit easier excitation by a semiconductor diode laser. Emission from the $^4F_{3/2}$ to $^4I_{11/2}$ multiplets was observed for seven different types of sites by site selective excitation, but the results are not directly comparable with the $^4F_{3/2}$ to $^4I_{9/2}$ fluorescence arising predominantly from a single type of site observed in the present work.

Raman/fluorescence spectra were obtained for one sample of natural powellite and are shown in Fig. 3. The spectra are very clean and transition assignments can be made for all seven peaks observed at 294 K and all eight peaks observed at 77 K. The resulting energy level values are given in the first and second data columns in Table 3.

Scheelite ($CaWO_4$)

Scheelite has a tetragonal crystal structure (space group $I4_1/a$) and the Ca^{2+} ions have tetragonal $\bar{2}$ (S_4) site symmetry. Fluorescence of Nd^{3+} in scheelite has been studied in connection with the use of scheelite as a laser host for Nd using $^4F_{3/2} \rightarrow {}^4I_{9/2}$ transitions. Varona et al. (2006) were able to construct energy-level diagrams of the five levels of the $^4I_{9/2}$ multiplet and two levels of the $^4F_{3/2}$ multiplet. Bayrakceken et al. (2007) were able to determine the energy level values for the $^4I_{9/2}$, $^4I_{11/2}$, $^4I_{13/2}$ and $^4I_{15/2}$ multiplets and compare them with theoretical values calculated from a crystal-field Hamiltonian for the S_4 tetragonal site symmetry using 11 parameters. The fit for the $^4I_{9/2}$ multiplet was relatively poor (rms deviation = 26.1 cm^{-1}) because the multiplets were considered individually and J-mixing was not included. However, the experimental values for the four higher levels of the $^4I_{9/2}$ multiplet obtained by the two groups agree closely and are shown in the first two data columns of Table 4.

Raman/fluorescence spectra were obtained for three samples of natural scheelite. The spectra of a sample of scheelite from Strawberry Mine in California are shown in Fig. 4. Six transitions can be identified at 294 K and eight at 77 K. The resulting energy level values are given in the third and fourth data columns of Table 4 and agree closely with those of the two previous groups. The unidentified lines near 1340 cm^{-1} (77 K) and 1850 cm^{-1} (77 K and 294 K) are probably due to Nd^{3+} transitions at sites of symmetry different from the normal S_4 symmetry.

297 **Comparison of powellite and scheelite**

298 A comparison of the spectra of powellite, shown in Fig. 3, and the spectra of
299 scheelite, shown in Fig. 4, reveals the following information:

300 1. The positions of the Nd^{3+} fluorescence peaks in scheelite occur at frequency
301 shifts that are 5-20 cm^{-1} lower than their counterparts in powellite.
302 2. The relative intensities of the fluorescence peaks are very similar in the two
303 sets of spectra. The correlation coefficient of the intensities is 0.91 at 294 K
304 and 0.93 at 77 K.

305 These results suggest a practical application of Raman/fluorescence spectra in
306 determining the relative content of molybdenum vs. tungsten in natural powellite-
307 scheelite rocks. Traditionally, visible fluorescence excited by shortwave UV radiation at
308 254 nm has been used for this purpose (Vermaas; Modreski, 1978). However, because the
309 fluorescence color changes quickly from bluish-white to yellow as the relative Mo
310 content rises to more than 5%, it is not very useful for distinguishing rocks whose Mo
311 content is in the range of 5-100%. In rocks containing rare-earth impurities, which are the
312 common case, the positions of the peaks in the Nd^{3+} fluorescence spectrum could be
313 used as a measure of the relative Mo/W content, which varied more linearly throughout
314 the entire range of 0% to 100%. Many more spectra with samples of different
315 compositions are needed to verify that the Raman/fluorescence spectra can indeed be a
316 reliable indicator of the relative Mo/W content.

317

318

319

320 **Apatite ($Ca_5(PO_4)_3(F, OH, Cl)$)**

321 Apatite has a hexagonal crystal structure (space group $P6_3/m$). The cation may be
322 F^- (fluorapatite), Cl^- (chlorapatite) or OH^- (hydroxylapatite) and is usually some mixture
323 of the three in natural minerals. There are two inequivalent sites for the Ca^{2+} ions in
324 apatite. The Ca I sites have trigonal *3* (C_3) symmetry and the Ca is surrounded by nine
325 oxygen ions which form three equilateral triangles. The Ca II sites have monoclinic *m*
326 (C_{1h}) symmetry and the Ca^{2+} is surrounded by six oxygen ions and one $F^-/Cl^-/OH^-$
327 ion. Most workers have assumed that because of ionic size constraints, Nd^{3+} substitutes
328 for the Ca^{2+} in the Ca II site.

329 Energy level schemes for Nd^{3+} in fluorapatite have been determined by both
330 Bruk et al. (1968), using both absorption and emission spectra, Kushida (1969) using
331 emission spectra, and by Gruber et al. (1996), using site selective excitation and polarized
332 absorption spectra. The three sets of results agree closely except for the Z_2 level value
333 from Bruk et al. (1968).

334 Raman/fluorescence spectra were obtained for four samples of apatite: one of
335 yellow apatite from Durango, Mexico, one of green apatite and two of blue apatite from
336 Madagascar. The chemical compositions of the yellow and green apatite samples were
337 determined by using a JEOL 7401 FESEM equipped with the EDAX GENESIS EDS
338 system. The atomic percentages of Ca, P, O and F+Cl were close to nominal, and the
339 Cl/F ratio was about 5%. The Si and REE concentrations were each about .5% and no
340 measurable Na was detected. The results strongly indicate that all four apatite samples are
341 dominantly fluorapatite with REE impurities charge-compensated by Si^{4+} substituting for

342 P^{5+}. The results are consistent with the picture given by Ransbo (1989) and Hughes et al.
343 (1991), in which, in natural apatite, Nd^{3+} can substitute equally well at either Ca site, and
344 charge balance is maintained by either $Si^{4+} \Rightarrow P^{5+}$ or $Na^{+} \Rightarrow Ca^{2+}$.

345 The Raman/fluorescence spectra of all four apatite samples share several common
346 features. First, Nd^{3+} fluorescence is the strongest of any of the minerals studied in this
347 work and is consistent with the high levels of Nd concentration detected by the LA-ICP-
348 MS method shown in Fig. 6. Second, the peak positions of the fluorescence lines agree
349 closely to within a few cm^{-1}. Only the relative intensities are sometimes different. Third,
350 the peak positions do not correspond to those that would be predicted by the energy level
351 scheme mentioned above but occur at values of frequency shift lower by 100-300 cm^{-1}.
352 Fourth, although the lines sharpen somewhat at 77 K, it is not possible to make transition
353 assignments.

354 The origin of the different Nd^{3+} fluorescence spectra is very probably due to the
355 different charge-compensating mechanisms and site occupancies in synthetic and natural
356 apatite. Most studies of Nd^{3+} fluorescence in apatite have been done on synthetic
357 samples. Mackie and Young (1973) concluded that Nd^{3+}site occupancy depends on the
358 doping vehicle. The use of Nd_2O_3 forces the Nd^{3+} to occupy Ca II sites exclusively. In
359 natural apatite both Ca I and Ca II sites may be occupied.

360 Further study with both natural and synthetic apatite will help to clarify the
361 different types of Nd^{3+} fluorescence spectra which can occur. However, even if the
362 charge-compensation mechanism is restricted to Si^{4+}substituting for P^{5+} in an adjacent P
363 site, there are six different possible crystal field environments for Nd^{3+} in natural apatite.

Thus the fluorescence lines are inherently broader, and the fluorescence spectra are more difficult to interpret.

Grossular/tsavorite ($Ca_3Al_2Si_3O_{12}$)

Grossular has a cubic crystal structure (space group $Ia\bar{3}d$) and the Ca^{2+} ions have orthorhombic *222* (D_2) site symmetry. Tsavorite is a form of the garnet grossular having a green color due to trace amounts of chromium and/or vanadium substituting for aluminum. Most tsavorite comes from the Tsavo region in Kenya and it is widely used as a gemstone.

Raman/fluorescence spectra were obtained for two samples of grossular and two samples of tsavorite. The spectra for one of the samples of tsavorite are shown in Fig. 5. The main difference between the two sets of spectra is that the intensity of the Nd^{3+} fluorescence lines, relative to that of the Raman lines, is about ten times larger in the tsavorite samples. In the region of frequency shifts from 1000 cm^{-1} to 2500 cm^{-1} eight strong Nd^{3+} fluorescence lines are observed at 294 K. As the temperature is lowered, the three lines at 1118/1112 cm^{-1}, 1360/1357 cm^{-1}, and 2024/2025 cm^{-1} show a strong decrease in intensity while the other four lines show an increase. All lines get narrower.

Although the spectra of Nd^{3+} in grossular and tsavorite have not been reported in the literature previously, tentative transition assignments for the lines may be made under the following three assumptions:

1. The three lines which are significantly weaker at 77 K are due to transitions from the R_2 level, which is depopulated at 77 K by more than an order of magnitude.

2. The other four lines are due to transitions from the R_1 level.

3. The separation between the R_1 and R_2 levels is in the range of 100-200 cm^{-1}, which is comparable with that of other materials.

The energy levels of Nd^{3+} in tsavorite deduced from this transition-assignment scheme are given in the third and fourth columns of Table 3. The scheme nicely explains all of the fluorescence lines except for the shoulder at 1541/1532 cm^{-1} on the low-frequency-shift side of the most intense line due to $R_1 \rightarrow Z_1$. This shoulder is most likely due to the $R_1 \rightarrow Z_1$ transition at sites of slightly different symmetry than the dominant (presumably *222 (D_2)*) site symmetry.

The fluorescence spectra of Nd^{3+} in grossular and tsavorite are the cleanest and most reliable indicator of the host material of those for the six minerals studied in this work. Owing to the greater crystal-field splitting of the R_1 and R_2 levels and larger depopulation of R_2 at 77 K, the spectra are also the easiest to interpret. Although crystal field calculations have not yet been performed for Nd^{3+} in grossular or tsavorite, they have been done for Nd^{3+} in garnets used for laser hosts (Gruber et al., 1990). For these minerals the R_2 - R_1 difference is most sensitive to the strength of the crystal field parameters B_2^0 and B_2^2.

Raman lines

Although the main topic of this paper is Nd^{3+} fluorescence in the six minerals chosen for study, at least one Raman line is present in the Raman/fluorescence spectra of five of them, i.e. all except apatite. In addition, a significant change of frequency shift

409 with temperature occurs in both fluorite and calcite. Because the spectra presented in
410 Fig. 2 through Fig. 5 start at 1000 cm^{-1} in order to display the Nd^{3+} fluorescence lines
411 clearly, most of these Raman lines are not shown. However, their frequency shifts and
412 changes with temperature are briefly discussed in this subsection and compared with the
413 results of other workers. Measurement and analysis of the Raman spectra of the five
414 minerals is given by Russell (1965) for fluorite, Rutt and Nicola (1974) and Herman et
415 al. (1987) for calcite, Crane et al. (2002) and Manjon et al (2006) for scheelite, Leroy et
416 al. (2000) for apatite, and Kolesov (1998) for grossular.

417 Of the six minerals, fluorite has the simplest structure and has a single Raman-
418 active T_{2g} mode at 322 cm^{-1}. The other minerals have more complex structures and all
419 contain molecular complexes, i.e. CO_3^{-2}, WO_4^{-2}, PO_4^{-3} and SiO_4^{-4}, which act as a unit in
420 many of the vibrational modes. The modes can be divided into external modes, which
421 involve motion of the cation with respect to the molecular complex, and internal modes,
422 which involve motion within the molecular complex. The mode frequencies of the two
423 groups separate fairly cleanly. External/internal mode frequencies generally lie
424 below/above 400 cm^{-1}.

425 The theory of the temperature dependence of the frequencies of Raman modes
426 has been given by Balkanski et al. (1983) and Menindez and Cardona (1984). More
427 recent results on semiconducting materials are given by Gasanly et al. (1999) and Sarswat
428 et al. (2011) and the references cited therein. The temperature dependence of Raman
429 mode frequencies consists of two parts: a contribution due to thermal expansion and a
430 contribution due to anharmonic coupling to phonons of other branches. The thermal-
431 expansion term may be either positive (ω increases as T increases) or negative (ω

decreases as *T* increases). The anharmonic term is always negative and is usually the larger of the two. Although there do not exist many published results on the temperature dependence of Raman-mode frequencies in materials containing molecular complexes, it would be expected that the changes with temperature should be larger for the external modes than for the internal modes, owing to the stronger anharmonic coupling to other modes.

In the present work, in fluorite, the frequency of the T_{2g} mode is observed to decrease by 3 cm^{-1} (328 cm^{-1} to 325 cm^{-1}) as the temperature is raised from 77 K to 294 K, yielding an average slope of $1.3*10^{-2}$ cm^{-1}/K, a value compatible with that obtained by Mujaji and Comins (2007) at higher temperature. In calcite, the frequency of the external vibrational E_g mode decreases by 4 cm^{-1} (288 cm^{-1} to 284 cm^{-1}), an amount comparable to that measured by Sood et al. (1981). In contrast, those of the internal E_g and A_{1g} modes remain unchanged at 710 cm^{-1} and 1085 cm^{-1}, respectively. Similarly, the frequencies of the internal A_g mode in scheelite and the internal A_{1g} mode in tsavorite remain unchanged at 911 cm^{-1} and 880 cm^{-1}, respectively. These results clearly indicate that the expected larger change of mode frequency with temperature for the external modes is correct. However, further studies of these minerals with a different laser wavelength and much reduced Nd^{3+} fluorescence intensity will be required in order to determine the degree of temperature dependence for the large number of external and internal modes.

Temperature dependence of energy levels and linewidths

The energy levels of an impurity ion such as Nd^{3+} in a host crystal are governed by the local crystal field produced by both static strain and dynamic strain associated with lattice vibrations. It is the dynamic strain which causes temperature-dependent shifts of the energy levels and fluorescence lines and broadenings of the linewidths. Kushida (1969) reviewed the theory of these phenomena, measured fluorescence spectra of Nd^{3+} in both yttrium aluminum garnet (YAlG) and fluorapatite (FAP) from 4.2 K to 500 K, and compared the results with theoretical predictions.

The theoretical expression for the shift of energy levels includes both direct (single- phonon) and Raman (multiphonon) terms. Among the lower-lying levels, there are more higher-lying levels for a given level than lower-lying ones so the energy-difference denominators appearing in the Raman term tend to be negative. If the Raman term is dominant, most energy levels are lowered in energy and the higher-lying ones are lowered more because the energy-difference denominators are smaller. Thus, most spectral lines show a redshift as the temperature is raised. Kushida's results bore out this prediction, where, among the $R_m \rightarrow Z_n$ transitions, only $R_1 \rightarrow Z_5$ showed a blueshift.

Table 5 gives the changes in energy levels from 77 K to 294 K for the four minerals of the present work for which most energy levels could be determined, as well as an overall average for the four. The chief prediction of the theory, namely that, as the temperature is raised, the higher-lying levels within a multiplet are lowered more and that most fluorescent lines show redshifts is clearly obeyed. Clear blueshifts occur only for the $R_1 \rightarrow Z_5$ transition.

476 The theoretical expression for the linewidths includes a temperature-independent
477 term due to inhomogeneous strain broadening, as well as direct and Raman terms. In
478 Kushida's work the linewidths of most transitions ranged from 4 cm^{-1} to 16 cm^{-1} at low
479 temperatures and increased by 25-50% at 300 K. The exceptions were transitions to the
480 Z_1 level in YAlG, whose linewidths were less than 1 cm^{-1}. This difference results from
481 the fact that in YAlG, unlike FAP and the five minerals listed in Table 5, charge
482 compensation is not necessary when Nd^{3+} substitutes for Y^{3+} and the inhomogeneous
483 strain broadening is very small. In the present work, the linewidths are somewhat larger
484 (8-16 cm^{-1} at 77 K and 20-30 cm^{-1} at 300 K), most likely due to somewhat greater
485 inhomogeneous strain broadening as the result of charge compensation.
486

487 **RARE-EARTH CONCENTRATIONS AND CORRELATION WITH**
488 **FLUORESCENCE**

489 **Rare-earth concentrations**

490 Among the rare earth elements the isotopes chosen for determining the trace-
491 element concentrations were as follows: ^{139}La, ^{140}Ce, ^{141}Pr, ^{145}Nd, ^{146}Nd, ^{147}Sm,
492 ^{151}Eu, ^{155}Gd, ^{156}Gd, ^{157}Gd, ^{160}Gd, ^{159}Tb, ^{163}Dy, ^{165}Ho, ^{166}Er, ^{139}Tm, ^{169}Yb and ^{175}Lu.
493 Because Nd was particularly important in this study, both ^{145}Nd and ^{146}Nd were used as
494 a check on the accuracy of the method. The concentration values determined from the
495 two isotopes agreed closely for all samples except for the sample of BaF_2, probably due
496 to Ba+B (from the glass) masquerading as ^{146}Nd. In this case the lower concentration
497 value obtained from ^{145}Nd was used. In addition, Ba+O masqueraded as ^{151}Eu, ^{155}Gd and
498 ^{156}Gd.

499 Fig. 6 through Fig. 8 show the rare-earth-element (REE) concentration patterns
500 for five minerals, normalized to chondrite to eliminate the variation with the odd/even
501 atomic number and to create smooth curves. The only significant departures from
502 smoothness are the negative Ce anomaly in the powellite, and the negative Eu anomaly,
503 which is strong in the yellow apatite and weaker in the powellite, grossular and tsavorite.
504 Fig. 6 shows the REE concentration patterns for two of the samples of apatite and
505 the purified sample of CaF_2. The pattern for the apatite is heavy-rare-earth-element-
506 (HREE-) enriched by a factor of 2.5 relative to the standard pattern for Durango apatite
507 and has a very strong Eu anomaly. The other two samples from Madagascar give patterns
508 that are very close to the one shown for the blue apatite. The REE concentration values
509 measured for the apatite samples are the highest for any of the six minerals studied in this
510 work. The high Nd concentration correlates qualitatively with the high values of the
511 Nd^{3+} fluorescence intensity, which was so strong in these samples that the Raman lines
512 were not observable. For the fluorite sample the purification process has apparently taken
513 an originally light-rare-earth-element- (LREE-) enriched pattern and preferentially
514 reduced the LREE content, leaving it middle-rare-earth-element- (MREE-) enriched.
515 However, even a residual concentration of Nd (≈ 1 ppm) is enough to cause strong
516 fluorescence.
517 Fig. 7 shows the REE concentration patterns for samples of powellite and
518 scheelite. The powellite curve exhibits a typical LREE-enriched pattern with significant
519 negative Ce and Eu anomalies. The scheelite curve coming from a clear crystallite (≈ 1
520 mm size) embedded in a larger rock from Strawberry Mine, CA is remarkably similar to
521 that of the artificially purified fluorite sample.

This is a preprint, the final version is subject to change, of the American Mineralogist (MSA)
Cite as Authors (Year) Title. American Mineralogist, in press.
(DOI will not work until issue is live.) DOI: http://dx.doi.org/10.2138/am.2014.4311

Fig. 8 shows the REE concentration patterns for samples of grossular and tsavorite. The tsavorite curve is significantly LREE-depleted relative to that for grossular, even though the mineral ($Ca_3Al_2Si_2O_{12}$) is identical, indicating different conditions of formation. Comparing these two samples, the Nd^{3+} fluorescence intensity (relative to that of the Raman lines) is ten times stronger in the tsavorite, whereas the Nd concentration is about the same. An important factor may be iron, whose concentration is 50 times higher in the grossular sample and is known to have an inhibiting effect on the Nd^{3+} fluorescence (See below.).

Correlation of Nd^{3+} fluorescence with Nd concentration

The Nd^{3+} fluorescence intensity at 1140 cm^{-1}, plotted vs. measured Nd concentration on a log-log plot, is shown for the six synthetic fluoride samples in Fig. 9. Except for the sample of CaF_2: .05% Dy^{2+}, the data points can be closely fit by a straight line with a slope of 1.6, indicating that Nd^{3+} fluorescence intensity increases as Nd concentration to a power greater than one at concentration levels less than a few ppm. At higher concentration levels of Nd occurring in the other minerals ($\approx 10^3$ ppm), the Nd^{3+} fluorescence is only several times stronger than the highest levels shown in Fig. 9, suggesting that, for any mineral, the curve eventually bends over due to concentration quenching. The data for the sample of BaF_2 show that Nd^{3+} fluorescence can occur in non-calcium-based minerals, but is likely to be much weaker due to the poor match of ionic radius and lower incorporation of Nd^{3+}.

RAMAN/FLUORESCENCE SPECTRA II

UML and RRUFF spectra for six minerals

In order to get some idea of how common Nd^{3+} fluorescence is in both calcium-based and non-calcium-based minerals, a larger number of samples than those used in the current experiments is required. One of the leading on-line sources for Raman spectra is rruff.info/ which contains Raman spectra obtained with lasers of various wavelengths for hundreds of minerals and thousands of individual samples. The Raman spectra of greatest interest to the current work are the ones presented second in the RRUFF format, namely the ones entitled 'Broad Scan with Spectral Artifacts', in which the exciting laser wavelength is 785 nm or 780 nm. The RRUFF spectra taken with a 785-nm laser can be used directly to obtain peak positions of the Nd^{3+} fluorescence lines, which can be compared with those of the UML samples. RRUFF spectra taken with a 780-nm laser must first undergo a correction of -75 cm^{-1}.

Of the six minerals studied in the present work, the peak positions and relative intensities of fluorescence lines measured from RRUFF spectra agree fairly well with those of the UML spectra for four minerals, namely fluorite, powellite, scheelite, and grossular/tsavorite. For calcite and apatite, there is considerably more disagreement. Clearly, the variability of the Nd^{3+} fluorescence spectra is larger in the latter two minerals.

Occurrence of Nd^{3+} fluorescence in minerals

The Raman/fluorescence spectra of a much larger group of minerals available on the RRUFF website were examined for the presence of Nd^{3+} fluorescence in the

568 frequency-shift range of 1000-2500 cm^{-1} and rated on a qualitative scale: zero, very
569 weak, weak, moderate, strong, very strong, where strong denotes an intensity exceeding
570 that of the strongest Raman lines. A summary of the Nd^{3+} fluorescence in the six
571 minerals studied in the present work, taken from the RRUFF database, is given in
572 Table 6. The occurrence of strong or very strong Nd^{3+} fluorescence in a larger group of
573 minerals is summarized in Table 7 for calcium-based minerals and in Table 8 for non-
574 calcium-based ones.

575 Of the thirteen groups of calcium-based minerals listed in Table 7, the majority
576 (seven) exhibit a high occurrence of fluorescence, two exhibit a low occurrence and four
577 exhibit no fluorescence at all. Generally, the occurrence of fluorescence is consistent
578 within a group, the three exceptions being andradite (garnet group), hedenbergite
579 (pyroxene group) and zoisite (epidote group). Andradite and hedenbergite both contain
580 iron as a constituent and the presence of iron quenches the fluorescence as discussed
581 below. Of the four groups of non-calcium-based minerals listed in Table 8, only one
582 shows even a low occurrence of fluorescence, and for the other three it is either very low
583 or non-existent. Clearly the presence of calcium in the host material and more likely
584 incorporation of Nd^{3+} impurities is a strong determining factor in the occurrence of
585 Nd^{3+} fluorescence.

586 Table 9 summarizes the results for the five minerals which contain iron as a
587 major constituent. There is absolutely no evidence for any Nd^{3+} fluorescence in any of
588 the 46 samples. The mechanism of this fluorescence quenching by the iron is not
589 presently understood and deserves further investigation.

590

IMPLICATIONS

In Raman spectroscopy, the 785-nm titanium sapphire laser is often used instead of a visible laser to reduce unwanted fluorescence. Because Nd^{3+} contains fluorescing levels easily excited by 785 nm, and because Nd frequently occurs as a trace element in many common minerals, Nd^{3+} fluorescence is widespread, particularly in calcium-based minerals. Although there is some variation in the positions of the fluorescence lines due to different crystal field strengths, they usually lie in the range of Raman shifts of 1000 cm^{-1} to 2500 cm^{-1}. Workers using 785-nm excitation should be aware that structure observed in this range of Raman shift may not belong to the true Raman spectrum but may be due to Nd^{3+} fluorescence. Although it is not part of the Raman spectrum, the Nd^{3+} fluorescence has potential uses in three areas.

In mineral identification, the Nd^{3+} fluorescence spectra, like the Raman spectra, are often clean, reliable and distinctive enough to serve as an identifier of the host mineral, e.g. fluorite, powellite, scheelite and grossular/tsavorite in this work. In solid solutions such as powellite-scheelite, the positions of the fluorescence lines could be used to determine the relative proportion of the elements, e.g. molybdenum vs. tungsten. In some minerals containing a large amount of disorder, such as cubic zirconia, in which the Raman spectrum does not contain sharp lines, the Nd^{3+} fluorescence may be a more reliable identifier of the mineral.

In structure characterization, the sharpness of the Nd^{3+} fluorescence lines is a measure of the uniformity of the crystal and the homogeneity of the impurity sites. In this work the greatest variation of linewidth occurred in calcite. In some samples, at low temperature, the fluorescence lines became narrower than the instrument resolution,

614 whereas in others they remained broad. These results clearly warrant further studies of a
615 large number of samples with a high-resolution Raman spectrometer and correlation with
616 other methods of structure characterization.

617 In the determination of trace-element concentration, the intensity of the Nd^{3+}
618 fluorescence provides a quick and non-destructive method of estimating the Nd
619 concentration level. From this value the concentration levels of the other rare-earth
620 elements may often be estimated as well, since minerals having a similar origin often
621 have similar rare-earth-element concentration patterns. Because fluorescence intensity
622 depends on many factors, such as the concentration of quenching elements like iron, this
623 method is currently semi-quantitative, but its accuracy may be improved with a more
624 complete characterization of the mineral and its impurity content.

625

626

627

628 **ACKNOWLEDGEMENTS**

629 The authors would like to thank Prof. Mengyan Shen of UMass Lowell for the use of
630 the RSI-3000 Raman spectrometer. They would like to thank Prof. Katherine Kelley and
631 Marian Lytle at the Graduate School of Oceanography at the University of Rhode Island
632 for help in running the LA-ICP-MS system and analyzing the data. They would also like
633 to thank Prof. Nelson Eby of UMass Lowell for several informative discussions and Alex
634 Erlwein and Alaa Alfailakawi of UMass Lowell for help in preparing the manuscript.

635
636

637

REFERENCES CITED

Balkanski, M., Wallis, R.F., and Haro, E. (1983) Anharmonic effects in light scattering due to optical phonons in silicon. Physical Review B, 28, 1928

Bayrakceken, F., Demir, O. J., and Karaaslan, I. S. (2007) Specific heat functions for the orthorhombic Nd^{3+} in scheelite type of crystals. Spectrochimica Acta Part A, 66, 1291-1294.

Bruk, A.M., Yu K., Voron'ko, G.V.,Maksimova, V.V., Osiko, A.M. Prokhorov, K.F.,Shpilov, K.F., and Shcherbakov, I. A. (1968) Optical properties and stimulated emission of Nd^{3+} in fluor-apatite. ZhETF Pis. Red 8, No. 7, 357-360.

Crane, M., Frost, R.L., William, P.A. and Kloprogge, J.T. (2002) Raman spectroscopy of the molybdate minerals chillagite (tungsteinian wulfenite –I4), stolzite, scheelite, wolframite and wulfenite. Journal of Raman Spectroscopy, 33, 62-66.

Devanarayanan, G. , Morell, G. and Katiyar, R.S. (1991) Raman spectroscopy of BeO at low temperatures. Journal of Raman Spectroscopy, 22, 311-314.

Freeth, C.A. and Jones, G. D. (1982) Zeeman infrared spectra of calcium and strontium fluoride crystals containing cerium and neodymium. Journal of Physics C: Solid State Physics, 15, 6833-6849.

Gasanly, N.M. , Ozkan, H., Aydinli, A. and Yilmaz, I. (1999) Temperature dependence of the Raman-active phonon frequencies in indium sulfide. Solid State Communications, 110, 231-236.

Goldschmidt, V.M. (1926) Geochemische Verteilungsgesetze der Elemente. Skrifter Norske Videnskaps – Akad. Oslo, (I) Mat. Natur.

665 Gruber, J.B. , Hills, M.E. , Allik, T.H. Jayasankar, C.K. , Quaglino, J.R., and Richardson, F.S.(1990)
666 Comparative analysis of Nd^{3+} ($4f^3$) energy levels on four garnet hosts. Physical Review B., 41,
667 7999-8012.
668
669 Gruber, J.B., Morrison, C.A., Seltzer, M.D., Wright, A.O., Nadler, M.P., Allik, T.H., Hutchinson, J.A. and
670 Chai, B.H. (1996) Site-selective excitation and polarized absorption spectra of Nd^{3+} in
671 $Sr_5(PO_4)_3F$ and $Ca_5(PO_4)_3F$. Journal of Applied Physics, 79, 1746-1758.
672
673 Hermon, R.G., Bogdan, C.E., Sommer, A.J. and Simpson, D.R. (1987) Discrimination among carbonate
674 minerals by Raman spectroscopy using the laser microprobe. Applied Spectroscopy, 41, 437-440.
675
676 Hughes, J.M., Cameron, M. and Mariano, A. N. (1991) Rare-earth-element ordering and structural
677 variations in natural rare-earth-bearing apatites. American Mineralogist, Volume 76, pages 1165-
678 1173.
679
680 Jenkins, A. L. and Larsen, R. A. (2004) Gemstone identification using Raman spectroscopy. Spectroscopy,
681 19(4), 20-25.
682
683 Kelley, K. (2006) A tutorial on the treatment of time resolved laser-ablation ICP-MS data. GSO/URI
684 internal report.
685
686 Kiss, Z. J.(1962) Crystal field splitting in $CaF_2 : Nd^{3+}$, Journal of Chemical Physics, 38, 1476-1480.
687
688 Kolesov, B. A. and Geiger, C.A. (1998) Raman spectra of silicate garnets. Physics and Chemistry of
689 Minerals, 25, 142-151.
690

691 Kushida, T. (1969) Linewidths and thermal shifts of spectral lines in neodymium-doped yttrium aluminum
692 garnet and calcium fluorophosphate. Physical Review, 185, 500-508.
693
694 Leroy, G., Leroy, N., Penel, G., Rey, C., Lafforgue, P. and Bres, E. (2000) Polarized micro-Raman study
695 of fluorapatite single crystals. Applied Spectroscopy, 54, 1521-1527.
696
697 Mackie, P.E. and Young, R. A. (1973) Location of Nd dopant in fluorapatite, $Ca_5(PO_4)_3F$: Nd. Journal of
698 Applied Crystallography, 6, 26-31.
699
700 Manjon, F. J., Errondonea, D., Garro, N., Pellicer-Porres J., Rodriguez-Hernandez, P., Radescu, S. Lopez-
701 Solano, J., Mujica, A., and Munoz, A. (2006) Lattice dynamics study of scheelite tungstates under
702 high pressure I. $BaWO_4$. Physical Review B, 74, 144111-(1-17).
703
704 Modreski, P.j. (1978) Ultraviolet fluorescence of minerals: examples from New Mexico. New Mexico
705 Geology, 9, 25-30 & 42.
706
707 Mujaji, M. and Comins, J.D. (2007) A Raman study of the superionic behavior of CaF_2 crystals containing
708 trivalent lanthanide ions. Phys. Status Solidi, 4, 851-855.
709
710 Menendez, J. and Cardona, M. (1989) Temperature dependence of the first-order Raman scattering by
711 phonons in Si, Ge, and $\alpha-$Sn: Anharmonic effects. Physical Review B, 29, 2051.
712
713 Payne, S.A., Caird, J.A., Chase, L.L., Smith, L.K., Nielsen, N.D. and Krupke, W. F. (1991) Spectroscopy
714 and gain measurements of Nd^{3+} in SrF_2 and other fluorite-structure hosts. Journal of the Optical
715 Society of America B, 8, 726-740.
716

Ransbo, J.G. (1989) Coupled substitutions involving REEs and Na and Si in apatites in alkaline rocks from Ilimaussaq intrusion, South Greenland, and the petrological implications. American Mineralogist, 74, 896-901.

Russell, J.P.(1965) The Raman spectrum of calcium fluoride. Proceedings of the Physical Society, 85, 194-197.

Rutt, H. N. and Nicola, J. H. (1974) Raman spectra of carbonates of calcite structure. Journal of Physics and Chemistry of Solids, 7, 4522-4528.

Sarswat, P.K. , Free, M.L. , and Tiwari , A. (2011) Temperature-dependent study of the Raman A mode of Cu_2ZnSnS_4 thin films. Phys. Status Solidi B, 248, 2170-2174.

Sood, A.K., Arora, A.K., Umadevi, V. and Venkataraman, G. (1981) Raman study of temperature dependence of lattice modes in calcite. Pramana, 16, 1-16.

Varona, C., Loiseau, P., Aka, G. and Ferrand, B. (2006) New Nd-doped crystals designed for laser operation around 900 nm along the $^4F_{3/2} \rightarrow {}^4I_{9/2}$ channel. OSA/ ASSP 2006, WB19.

Vermaas, F. H. S, South Africa scheelites and an x-ray method for determining members of the scheelite-powellite series. Geological Survey, Pretoria, South Africa

.

Withers, S.H., Peale, R.E., Schulte, R.E., Braunstein, A.F., Beck, K.M., Hess, W.P. and Reeder, R.J. (2003) Broad distribution of crystal-field environments for Nd^{3+} in calcite. Physics and Chemistry of Minerals, 30, 440-448.

http://rruff.info/.

744
745
746
747
748
749
750
751
752
753
754
755
756
757
758
759
760
761
762
763

Figure Captions

764 **Figure 1.** The 4f^n energy-level structure for four trivalent rare earth ions (Nd^{3+}, Dy^{3+},
765 Er^{3+} and Ho^{3+}) all have absorption bands close to 785 nm (12739 cm^{-1}) but only Nd^{3+}
766 produces fluorescent lines shifted from 12739 cm^{-1} by 1000-2500 cm^{-1}.

767 **Figure 2.** Raman/fluorescence spectra of fluorite (CaF_2) at 294 K (top) and 77 K (bottom).
768 At 77 K all lines sharpen, two more transitions ($R_2 \rightarrow Z_1$ and $R_2 \rightarrow Z_3$) are visible, and the intensity
769 of $R_2 \rightarrow Z_5$ relative to that of $R_1 \rightarrow Z_5$ is significantly reduced due to depopulation of the R_2 level at
770 low temperature.

Figure 3. Raman/fluorescence spectrum of powellite ($CaMoO_4$) at 294 K (top) and 77 K (bottom). At 77 K all lines sharpen, one more transition ($R_1 \rightarrow Z_4$) is visible and the intensities of $R_2 \rightarrow Z_1/Z_3/Z_5$ relative to those of $R_1 \rightarrow Z_1/Z_3/Z_5$ are significantly reduced due to depopulation of the R_2 level at low temperature.

Figure 4. Raman/fluorescence spectrum of scheelite ($CaWO_4$) at 294 K (top) and 77 K (bottom). The spectra are very similar to those of powellite with the line positions shifted downward by 5-20 cm^{-1}.

Figure 5. Raman/fluorescence spectrum of tsavorite ($Ca_3Al_2Si_3O_{12}$) at 294 K (top) and 77 K (bottom). At 77 K all lines sharpen and the intensities of $R_2 \rightarrow Z_1/Z_3/Z_5$ relative to those of $R_1 \rightarrow Z_1/Z_3/Z_5$ are very strongly reduced due to the larger energy difference of the R_1 and R_2 levels and the very large depopulation of the R_2 level at low temperature.

Figure 6. Chondrite-normalized concentrations of rare-earth elements for fluorite and apatite. The apatite samples have the highest REE concentrations and both show a LREE-enriched pattern, with a weaker enrichment in the blue apatite. The pattern for the fluorite sample (manufactured not natural) is depleted in both LREEs and HREEs. All three curves exhibit an Eu anomaly which is strongest (a factor of four) in the yellow apatite.

Figure 7. Chondrite-normalized concentrations of rare-earth elements for powellite and scheelite. The pattern for powellite is LREE-enriched and shows a significant Eu anomaly. The pattern for scheelite (natural) is remarkably similar in both shape and absolute values to that for fluorite (manufactured) shown in Fig. 6.

Figure 8. Chondrite-normalized concentrations of rare-earth elements for grossular and tsavorite. Both patterns show a steeply declining depletion for the LREEs as well as a gradually declining depletion for the HREEs. A weak Eu anomaly is evident in both curves.

Figure 9. Nd^{3+} fluorescence vs. Nd concentration for fluoride samples. The dependence of Nd^{3+} fluorescence intensity on measured Nd concentration is approximately linear on a log-log plot ($I \sim n^{1.6}$) for four of the five samples shown. Data from other samples suggest that at higher concentration levels the curve bends over due to concentration quenching.

Tables

Table 1. Minerals chosen for study

UML Samples			
Mineral	# Samples	Color	Source or Origin
CaF_2	5	clear	Fairfield Crystal Technology, Optovac Inc.
	2	green	unknown
BaF_2	1	clear	Optovac Inc.
$CaCO_3$	1	green	unknown
	1	blue	unknown
	3	clear	unknown

$CaMoO_4$	1	yellow	St. Louis Claims, AZ
$CaWO_4$	1	clear	Strawberry Mine, CA
	1	clear	Trumbull, CT
	1	yellow	Emerald Lake, YU
$Ca_5P_3O_{12}F$	1	yellow	Durango, Mexico
	1	green	Madagascar
	2	blue	Madagascar
$Ca_3Al_2Si_3O_{12}$	2	yellow	Kenya
	2	green	Tanzania

816

RRUFF Samples			
Mineral	# Samples	Color	Source or Origin
CaF_2	2	green	Hunan Province, China
$CaCO_3$	1	clear	Durango, Mexico
$CaWO_4$	1	orange	Sonora, Mexico
$Ca_5P_3O_{12}F$	1	brown	Minas Gerais, Brazil
	1	clear	Kola Peninsula, Russia
$Ca_3Al_2Si_3O_{12}$	5	green	Wah Wah Mts. UT, Lolatema, Tanzania, Unknown, Mali

817
818
819
820

Table 2. Energy levels (cm^{-1}) of Nd^{3+} in fluorite as deduced from fluorescence spectra

Level	Kiss (1962)	Freeth and Jones (1980)	Payne et al (1990)	Present Work	
	294 K	294 K	294 K	77 K	294 K
R_2	-	11708	11705	11713	11703
R_1	11594	11596	11601	11600	11602
Z_5	784	746	738	747	740
Z_4	-	-	-	-	-
Z_3	212	201	210	201	206
Z_2	109	81 (77 K)	101	82	97
Z_1	0	0	0	0	0

Table 3. Energy levels (cm^{-1}) of Nd^{3+} in powellite and tsavorite as deduced from fluorescence spectra in the present work

Level	Powellite		Tsavorite	
	77 K	294 K	77 K	294 K
R_2	11463	11457	11632	11627
R_1	11394	11390	11435	11431
Z_5	461	455	917	912
Z_4	223	-	454	450
Z_3	166	166	255	254
Z_2	110	105	177	176
Z_1	0	0	0	0

Table 4. Energy levels (cm^{-1}) of Nd^{3+} in scheelite as deduced from fluorescence spectra

Level	Varona et al. (2006)	Bayrukgen et al. (2007)	Present Work	
	294 K	294 K	77 K	294 K
R_2	11480	-	11479	11475
R_1	11415	-	11412	11407
Z_5	475	471	474	463
Z_4	232	230	234	-
Z_3	160	161	163	159
Z_2	119	114	114	-
Z_1	0	0	0	0

Table 5. Change of energy levels of Nd^{3+} from 77 K to 294 K in four minerals

Level	Fluorite	Powellite	Scheelite	Tsavorite	Average
R_2	-10	-8	-4	-5	-6.8
R_1	2	-4	-5	-4	-2.8
Z_5	-7	-6	-11	-5	-7.3
Z_4	-	-	-	-4	-4.0
Z_3	5	0	-4	-1	0
Z_2	15	-5	-	-1	3.0
Z_1	0	0	0	0	0

Table 6. Summary of Raman/fluorescence spectra of six minerals from RRUFF

Chemical Formula	Number of Samples	Fluorescence						
		0	vw	w	m	s	vs	% s or vs
CaF_2	3	0	0	0	0	0	3	100
$CaCO_3$	12	7	3	0	0	0	2	17
$CaMoO_4$	2	1	0	0	0	0	1	50
$CaWO_4$	1	0	0	1	0	1	0	50
$Ca_5(PO_4)_3F$	17	0	0	2	0	1	14	88
$Ca_3Al_2Si_3O_{12}$	18	4	3	0	1	1	9	56

Table 7. Occurrence of strong or very strong Nd^{3+} fluorescence in RRUFF samples of calcium-based minerals listed by group

Range	Group	Number of Samples	% Occurrence
High ~50-100%	Fluorides	3	100
	Molybdates and Tungstates	3	67
	Phosphates	21	76
	Garnet group	20	60
	Olivine group	1	100
	Melilite group	6	50
	Pyroxene group	19	47
Low 10-25%	Carbonates	23	22
	Sulfates	15	13
Zero	Borates	4	0
	Epidote group	13	0
	Amphibole group	16	0
	Mica group	4	0

Table 8. Occurrence of strong or very strong Nd^{3+} fluorescence in RRUFF samples of non-calcium-based minerals listed by group

Range	Group	Number of Samples	% Occurrence
Low (10-25%)	Aragonite group	7	14
Very low (1-10%)	Calcite group	19	5
	Garnet group	34	3
Zero	Olivine group	31	0

Table 9. Occurrence of any Nd^{3+} fluorescence in RRUFF samples containing Fe

Ca Basis	Group	Mineral	Number of Samples	% Occurrence
Ca-based	Garnet group	Andradite	19	0
	Pyroxene group	Hedenbergite	4	0
Non-Ca-based	Calcite group	Siderite	5	0
	Garnet group	Almandine	11	0
	Olivine group	Fayalite	7	0

Figures

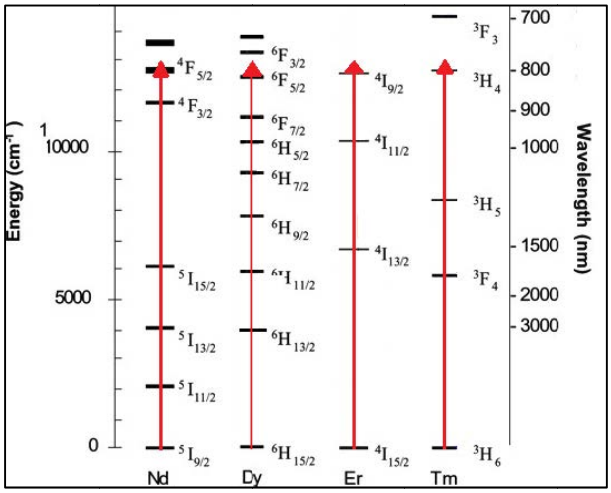

Figure 1 (4 rare earths)

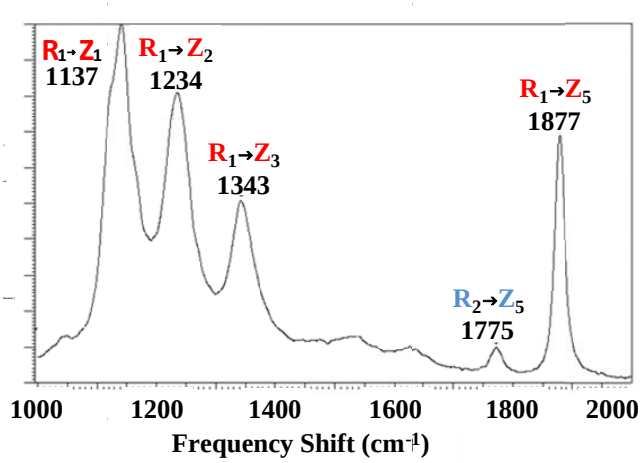

41

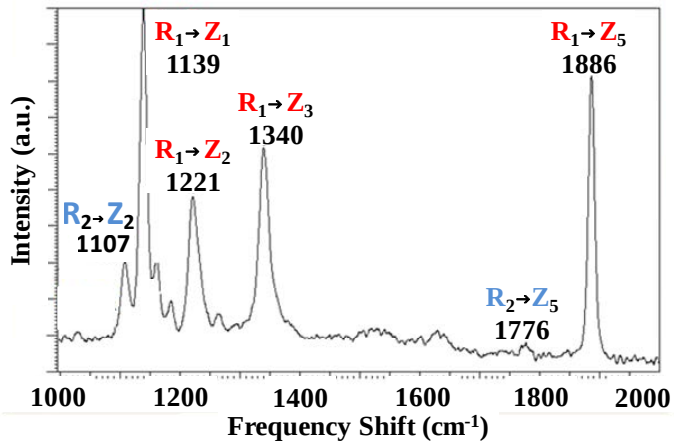

875
876
877 **Figure 2** (fluorite)

878

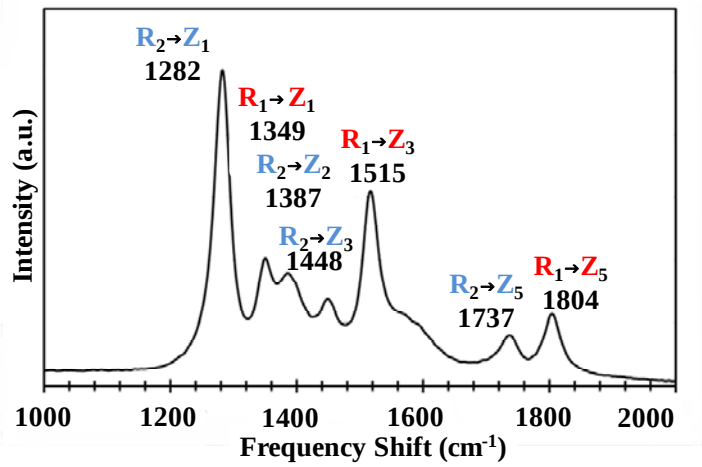

879

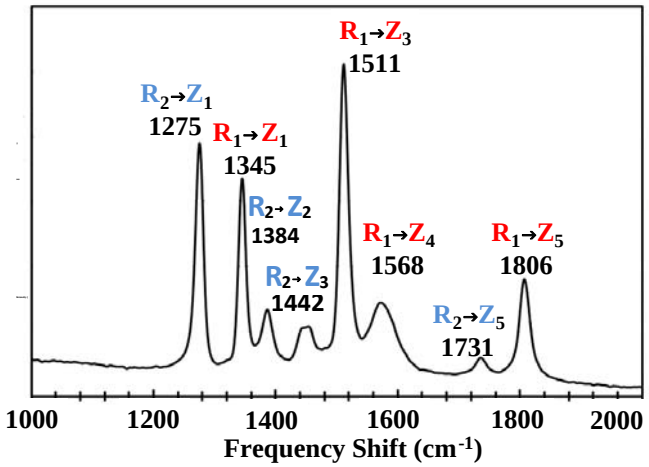

880
881
882
883 **Figure 3** (powellite)
884

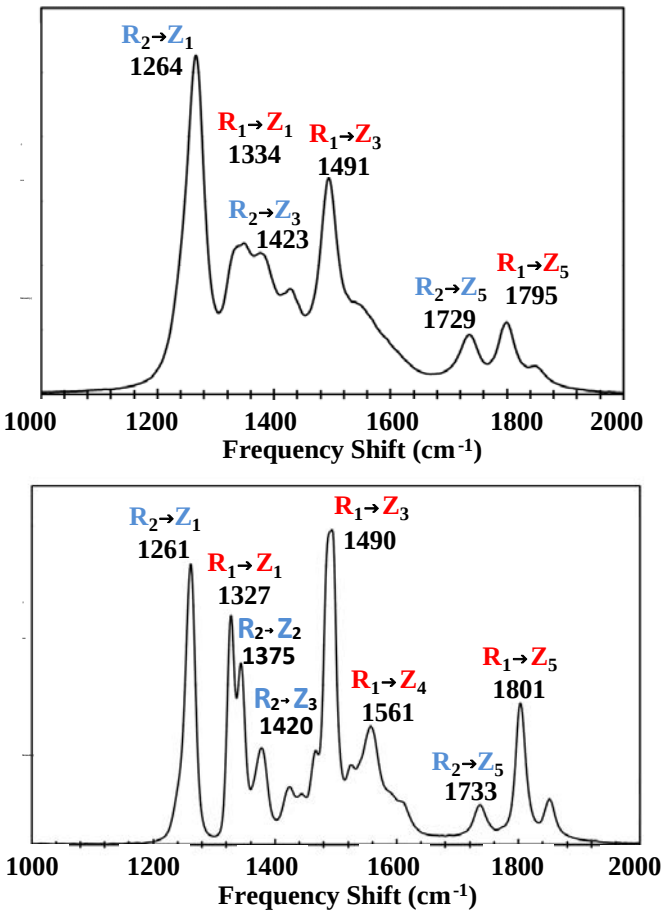

Figure 4 (scheelite)

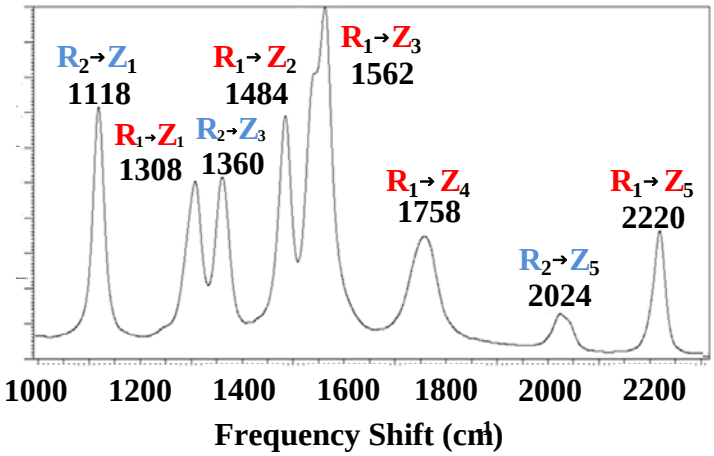

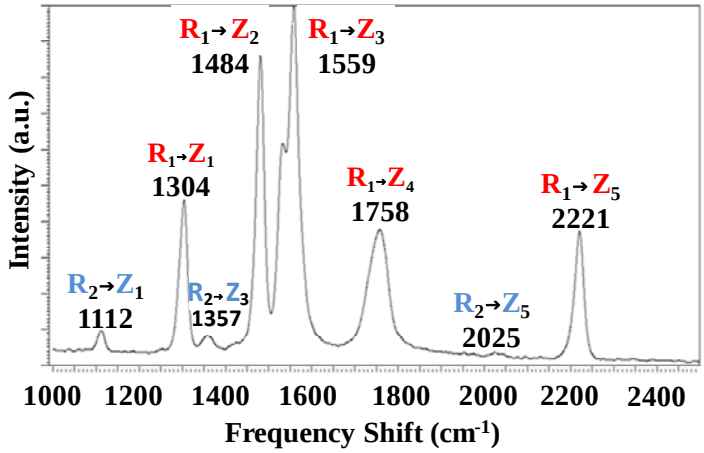

Figure 5 (tsavorite)

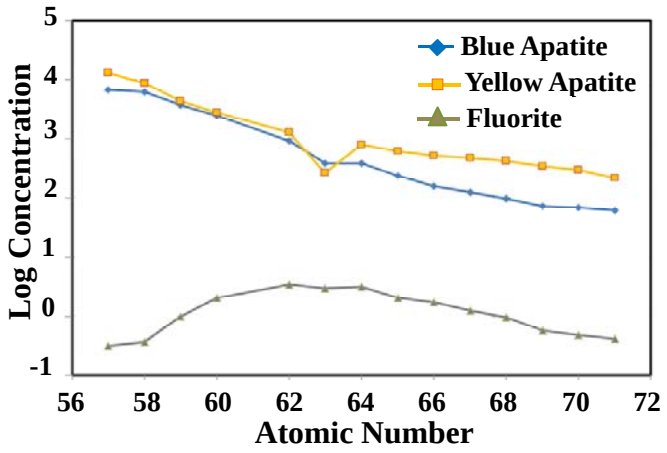

Figure 6 (apatite and fluorite)

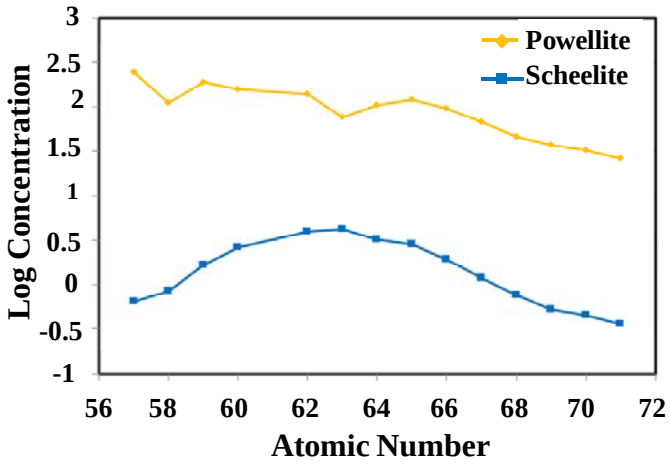

Figure 7 (powellite and scheelite)

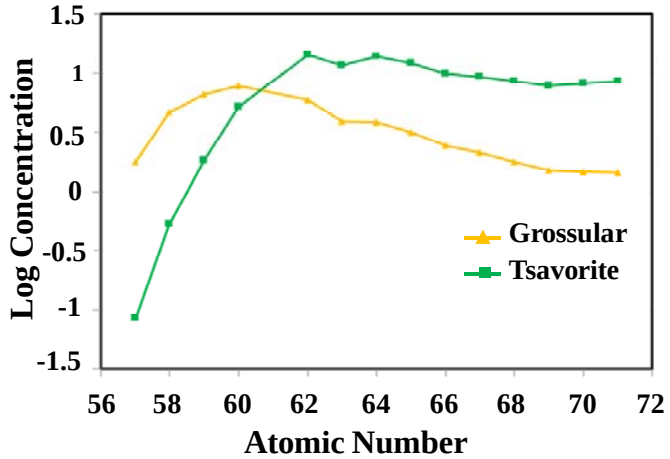

Figure 8 (grossular and tsavorite)

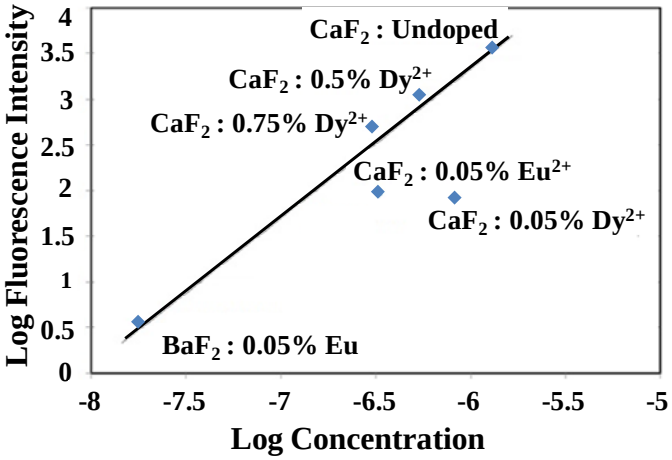

Figure 9 (fluorite)